

Ultra-broadband sum-frequency vibrational spectrometer of aqueous interfaces based on a non-collinear optical parametric amplifier

Oleksandr Isaienko and Eric Borguet*

Department of Chemistry, Temple University, 1901 North 13th Street, Philadelphia, Pennsylvania, USA
*eborguet@temple.edu

Abstract: We describe an ultrabroadband IR-visible sum-frequency (SF) setup that allows simultaneous acquisition of the entire vibrational spectrum of water molecules at mineral surfaces in the OH stretching region without ever tuning the IR laser pulses. Our newly developed 800-nm pumped noncollinear optical parametric amplifier (NOPA) generates broadband mid-IR pulses (~ 1800 – 3500 nm, or ~ 2900 – 6000 cm^{-1}) with bandwidths >600 cm^{-1} at half-maximum at near 3500 cm^{-1} . Using the ultra-broadband IR NOPA, we constructed a sum-frequency vibrational spectrometer that allowed the acquisition of spectra of the OH stretches of water at hydrophilic and hydrophobic silica surfaces, over the frequency range ~ 2900 – 3800 cm^{-1} , within 60 s, much shorter than with scanning SFG spectrometers. The ultra-broadband SFG spectrometer reported here can be potentially applied to time-resolved measurements of kinetics at interfaces.

©2011 Optical Society of America

OCIS codes: (190.4350) Nonlinear optics at surfaces; (190.4970) Parametric oscillators and amplifiers; (240.1485) Buried interfaces; (300.6490) Spectroscopy, surface.

References and links

1. Y. R. Shen and V. Ostroverkhov, "Sum-frequency vibrational spectroscopy on water interfaces: polar orientation of water molecules at interfaces," *Chem. Rev.* **106**(4), 1140–1154 (2006).
2. G. L. Richmond, "Molecular bonding and interactions at aqueous surfaces as probed by vibrational sum frequency spectroscopy," *Chem. Rev.* **102**(8), 2693–2724 (2002).
3. F. Vidal and A. Tadjeddine, "Sum-frequency generation spectroscopy of interfaces," *Rep. Prog. Phys.* **68**(5), 1095–1127 (2005).
4. M. S. Yeganeh, S. M. Dougal, and H. S. Pink, "Vibrational spectroscopy of water at liquid/solid interfaces: Crossing the isoelectric point of a solid surface," *Phys. Rev. Lett.* **83**(6), 1179–1182 (1999).
5. L. Zhang, C. Tian, G. A. Waychunas, and Y. R. Shen, "Structures and charging of alpha-alumina (0001)/water interfaces studied by sum-frequency vibrational spectroscopy," *J. Am. Chem. Soc.* **130**(24), 7686–7694 (2008).
6. M. Flörshheimer, K. Kruse, R. Polly, A. Abdelmonem, B. Schimmelpfennig, R. Klenze, and T. Fanghänel, "Hydration of mineral surfaces probed at the molecular level," *Langmuir* **24**(23), 13434–13439 (2008).
7. K. A. Becraft and G. L. Richmond, "In situ vibrational spectroscopic studies of the $\text{CaF}_2/\text{H}_2\text{O}$ interface," *Langmuir* **17**(25), 7721–7724 (2001).
8. A. J. Hopkins, S. Schrödle, and G. L. Richmond, "Specific ion effects of salt solutions at the CaF_2 /water interface," *Langmuir* **26**(13), 10784–10790 (2010).
9. Q. Du, E. Freysz, and Y. R. Shen, "Vibrational spectra of water molecules at quartz/water interfaces," *Phys. Rev. Lett.* **72**(2), 238–241 (1994).
10. K. C. Jena and D. K. Hore, "Variation of ionic strength reveals the interfacial water structure at a charged mineral surface," *J. Phys. Chem. C* **113**(34), 15364–15372 (2009).
11. S. W. Ong, X. L. Zhao, and K. B. Eisenthal, "Polarization of water-molecules at a charged interface: second harmonic studies of the silica/water interface," *Chem. Phys. Lett.* **191**(3-4), 327–335 (1992).
12. K. C. Jena, P. A. Covert, and D. K. Hore, "The effect of salt on the water structure at a charged solid surface: differentiating second- and third-order nonlinear contributions," *J. Phys. Chem. Lett.* **2**(9), 1056–1061 (2011).
13. Z. Yang, Q. F. Li, M. R. Gray, and K. C. Chou, "Structures of water molecules at solvent/silica interfaces," *Langmuir* **26**(21), 16397–16400 (2010).
14. S. Ye, S. Nihonyanagi, and K. Uosaki, "Sum frequency generation (SFG) study of the pH-dependent water structure on a fused quartz surface modified by an octadecyltrichlorosilane (OTS) monolayer," *Phys. Chem. Chem. Phys.* **3**(16), 3463–3469 (2001).

15. C. S. Tian and Y. R. Shen, "Structure and charging of hydrophobic material/water interfaces studied by phase-sensitive sum-frequency vibrational spectroscopy," *Proc. Natl. Acad. Sci. U.S.A.* **106**(36), 15148–15153 (2009).
16. S. Schrödle and G. L. Richmond, "Sequential wavelength tuning: dynamics at interfaces investigated by vibrational sum-frequency spectroscopy," *Appl. Spectrosc.* **62**(4), 389–393 (2008).
17. L. J. Richter, T. P. Petralli-Mallow, and J. C. Stephenson, "Vibrationally resolved sum-frequency generation with broad-bandwidth infrared pulses," *Opt. Lett.* **23**(20), 1594–1596 (1998).
18. A. Lagutchev, A. Lozano, P. Mukherjee, S. A. Hambrir, and D. D. Dlott, "Compact broadband vibrational sum-frequency generation spectrometer with nonresonant suppression," *Spectrochim. Acta A Mol. Biomol. Spectrosc.* **75**(4), 1289–1296 (2010).
19. S. Nihonyanagi, A. Eftekhari-Bafrooei, and E. Borguet, "Ultrafast vibrational dynamics and spectroscopy of a siloxane self-assembled monolayer," *J. Chem. Phys.* **134**(8), 084701 (2011).
20. A. B. Voges, G. Y. Stokes, J. M. Gibbs-Davis, R. B. Lettan, P. A. Bertin, R. C. Pike, S. T. Nguyen, K. A. Scheidt, and F. M. Geiger, "Insights into heterogeneous atmospheric oxidation chemistry: Development of a tailor-made synthetic model for studying tropospheric surface chemistry," *J. Phys. Chem. C* **111**(4), 1567–1578 (2007).
21. A. Eftekhari-Bafrooei and E. Borguet, "Effect of hydrogen-bond strength on the vibrational relaxation of interfacial water," *J. Am. Chem. Soc.* **132**(11), 3756–3761 (2010).
22. G. Ma, J. Liu, L. Fu, and E. C. Y. Yan, "Probing water and biomolecules at the air-water interface with a broad bandwidth vibrational sum frequency generation spectrometer from 3800 to 900 cm^{-1} ," *Appl. Spectrosc.* **63**(5), 528–537 (2009).
23. S. Nihonyanagi, S. Yamaguchi, and T. Tahara, "Direct evidence for orientational flip-flop of water molecules at charged interfaces: a heterodyne-detected vibrational sum frequency generation study," *J. Chem. Phys.* **130**(20), 204704 (2009).
24. S. Nihonyanagi, S. Ye, and K. Uosaki, "Sum frequency generation study on the molecular structures at the interfaces between quartz modified with amino-terminated self-assembled monolayer and electrolyte solutions of various pH and ionic strengths," *Electrochim. Acta* **46**(20-21), 3057–3061 (2001).
25. R. L. York, Y. M. Li, G. J. Hologing, and G. A. Somorjai, "Sum frequency generation vibrational spectra: the influence of experimental geometry for an absorptive medium or media," *J. Phys. Chem. A* **113**(12), 2768–2774 (2009).
26. E. Riedle, M. Beutter, S. Lochbrunner, J. Piel, S. Schenk, S. Sporlein, and W. Zinth, "Generation of 10 to 50 fs pulses tunable through all of the visible and the NIR," *Appl. Phys. B* **71**, 457–465 (2000).
27. D. Brida, C. Manzoni, G. Cirimi, M. Marangoni, S. Bonora, P. Villoresi, S. De Silvestri, and G. Cerullo, "Few-optical-cycle pulses tunable from the visible to the mid-infrared by optical parametric amplifiers," *J. Opt.* **12**(1), 013001 (2010).
28. T. Kobayashi and A. Shirakawa, "Tunable visible and near-infrared pulse generator in a 5 fs regime," *Appl. Phys. B* **70**, S239–S246 (2000).
29. C. J. Fecko, J. J. Loparo, and A. Tokmakoff, "Generation of 45 femtosecond pulses at 3 μm with a KNbO_3 optical parametric amplifier," *Opt. Commun.* **241**(4-6), 521–528 (2004).
30. I. Nikolov, A. Gaydardzhiev, I. Buchvarov, P. Tzankov, F. Noack, and V. Petrov, "Ultrabroadband continuum amplification in the near infrared using BiB_3O_6 nonlinear crystals pumped at 800 nm," *Opt. Lett.* **32**(22), 3342–3344 (2007).
31. D. Brida, C. Manzoni, G. Cirimi, M. Marangoni, S. De Silvestri, and G. Cerullo, "Generation of broadband mid-infrared pulses from an optical parametric amplifier," *Opt. Express* **15**(23), 15035–15040 (2007).
32. D. Brida, M. Marangoni, C. Manzoni, S. D. Silvestri, and G. Cerullo, "Two-optical-cycle pulses in the mid-infrared from an optical parametric amplifier," *Opt. Lett.* **33**(24), 2901–2903 (2008).
33. T. Fuji and T. Suzuki, "Generation of sub-two-cycle mid-infrared pulses by four-wave mixing through filamentation in air," *Opt. Lett.* **32**(22), 3330–3332 (2007).
34. P. B. Petersen and A. Tokmakoff, "Source for ultrafast continuum infrared and terahertz radiation," *Opt. Lett.* **35**(12), 1962–1964 (2010).
35. E. Rubino, J. Darginavicius, D. Faccio, P. Di Trapani, A. Piskarskas, and A. Dubietis, "Generation of broadly tunable sub-30-fs infrared pulses by four-wave optical parametric amplification," *Opt. Lett.* **36**(3), 382–384 (2011).
36. S. Cussat-Blanc, A. Ivanov, D. Lupinski, and E. Freysz, " KTiOPO_4 , KTiOAsO_4 , and KNbO_3 crystals for mid-infrared femtosecond optical parametric amplifiers: analysis and comparison," *Appl. Phys. B* **70**, S247–S252 (2000).
37. O. Isaienko and E. Borguet, "Generation of ultra-broadband pulses in the near-IR by non-collinear optical parametric amplification in potassium titanyl phosphate," *Opt. Express* **16**(6), 3949–3954 (2008).
38. O. Isaienko and E. Borguet, "Pulse-front matching of ultrabroadband near-infrared noncollinear optical parametric amplified pulses," *J. Opt. Soc. Am. B* **26**(5), 965–972 (2009).
39. O. Isaienko and E. Borguet, "Ultra-broadband infrared pulses from a potassium-titanyl phosphate optical parametric amplifier for VIS-IR-SFG spectroscopy," in *Ultrafast Phenomena XVI (Springer Series in Chemical Physics)*, P. Corkum, S. Silvestri, K. A. Nelson, E. Riedle, and R. W. Schoenlein, eds. (Springer Berlin Heidelberg, 2009), pp. 777–779.
40. O. Isaienko and E. Borguet, "Ultra-broadband near-IR non-collinear optical parametric amplification in potassium niobate and lithium niobate," in *Conference on Lasers and Electro-Optics/International Quantum*

Electronics Conference, OSA Technical Digest (CD) (Optical Society of America, 2009), paper CFC7.
<http://www.opticsinfobase.org/abstract.cfm?URI=CLEO-2009-CFC7>

41. O. Isaienko, E. Borguet, and P. Vöhringer, "High-repetition-rate near-infrared noncollinear ultrabroadband optical parametric amplification in KTiOPO₄," *Opt. Lett.* **35**(22), 3832–3834 (2010).
42. M. Tiihonen, V. Pasiskevicius, A. Fragemann, C. Canalias, and F. Laurell, "Ultra-broad gain in an optical parametric generator with periodically poled KTiOPO₄," *Appl. Phys. B* **85**(1), 73–77 (2006).
43. V. Petrov, F. Rotermund, and F. Noack, "Generation of high-power femtosecond light pulses at 1 kHz in the mid-infrared spectral range between 3 and 12 μm by second-order nonlinear processes in optical crystals," *J. Opt. A, Pure Appl. Opt.* **3**(3), R1–R19 (2001).
44. F. Rotermund, V. Petrov, and F. Noack, "Femtosecond noncollinear parametric amplification in the mid-infrared," *Opt. Commun.* **169**(1-6), 183–188 (1999).
45. D. Bodlaki and E. Borguet, "Picosecond infrared optical parametric amplifier for nonlinear interface spectroscopy," *Rev. Sci. Instrum.* **71**(11), 4050–4056 (2000).
46. A. Eftekhari-Bafrooei and E. Borguet, "Effect of surface charge on the vibrational dynamics of interfacial water," *J. Am. Chem. Soc.* **131**(34), 12034–12035 (2009).
47. W. J. Tropic, M. E. Thomas, and T. J. Harris, "Properties of crystals and glasses," in *Handbook of Optics*, 2nd ed., M. Bass, ed. (McGraw-Hill, New York, 1995), pp. 33.33–33.83.
48. T. J. Wang, Z. Major, I. Ahmad, S. A. Trushin, F. Krausz, and S. Karsch, "Ultra-broadband near-infrared pulse generation by noncollinear OPA with angular dispersion compensation," *Appl. Phys. B* **100**(1), 207–214 (2010).
49. G. Pretzler, A. Kasper, and K. J. Witte, "Angular chirp and tilted light pulses in CPA lasers," *Appl. Phys. B* **70**(1), 1–9 (2000).
50. N. Demirdöven, M. Khalil, O. Golonzka, and A. Tokmakoff, "Dispersion compensation with optical materials for compression of intense sub-100-fs mid-infrared pulses," *Opt. Lett.* **27**(6), 433–435 (2002).
51. C. Heese, L. Gallmann, U. Keller, C. R. Phillips, and M. M. Fejer, "Ultra-broadband, highly flexible amplifier for ultrashort midinfrared laser pulses based on aperiodically poled Mg:LiNbO₃," *Opt. Lett.* **35**(14), 2340–2342 (2010).

1. Introduction

Interfaces play a crucial role in the exchange of energy and matter in various physical, chemical and biological systems. Surface science significantly advanced with the introduction of second-order non-linear optical methods as the surface-sensitive probes in the 1980's [1–3]. Nonlinear optical phenomena such as second-harmonic generation (SHG) and sum-frequency generation (SFG) are forbidden, in the electric-dipole approximation, in media with inversion symmetry, such as isotropic solids, e.g., glass, or liquids, e.g., water. However, at the interface the inversion symmetry is lost (at least in the direction normal to the interface). This has made SHG and SFG indispensable tools for the characterization of various surfaces [1–3]. A common configuration, and the one used in our experiments, is the so-called visible-infrared SFG spectroscopy (VIS-IR SFG) which employs two laser beams: a beam in the frequency range of the vibrational transitions of interfacial oscillators (typically in the IR range, $\omega_{\text{IR}} \sim 1000 - 4000 \text{ cm}^{-1}$) and an off-resonant beam, ω_{VIS} , normally in the visible (VIS) range. The intensity of the sum-frequency signal ($\omega_{\text{SFG}} = \omega_{\text{IR}} + \omega_{\text{VIS}}$) $I_{\text{SFG}} \propto |\chi_{\text{eff}}^{(2)}|^2 I(\omega_{\text{IR}})I(\omega_{\text{VIS}})$ is measured as a function of ω_{IR} , where $I(\omega_{\text{IR}})$ and $I(\omega_{\text{VIS}})$ are the intensities of the input beams, and $\chi_{\text{eff}}^{(2)}$ is the effective second-order nonlinear susceptibility of the interface. As ω_{IR} approaches resonance with an active vibrational mode at the interface, the detected SF-signal enhances due to the frequency dependence of the surface nonlinearity [1–3]:

$$\chi_{\text{eff}}^{(2)} = \chi_{\text{NR}}^{(2)} + \sum_j \frac{B_j \exp(i\varphi_j)}{\omega - \omega_j + i\Gamma_j} \quad (1)$$

where $\chi_{\text{NR}}^{(2)}$ is the nonresonant susceptibility (typically caused by an instantaneous nonlinear electronic response); B_j – amplitude of j^{th} vibrational mode; Γ_j – natural linewidth of j^{th} vibrational mode; φ_j – phase of the j^{th} mode; ω_j – central frequency of j^{th} vibrational mode.

The importance of interfacial charging in various geochemical phenomena, such as metal ion adsorption/desorption, has motivated SFG-studies of various aqueous-mineral interfaces such as silica [1], alumina [4–6], calcium fluoride [7,8]. Since the pioneering SFG work by

the Shen group [9], the silica/water interface has been the subject of numerous studies [1,10–13]. Additionally, SFG spectroscopy has provided important information on modified surfaces, such as hydrophobic silica [14,15].

Even though vibrational SFG spectroscopy has been around for more than two decades, there still exist technical limitations, e.g., the narrow spectral bandwidth of the available IR laser sources (compared to non-laser IR sources used in linear IR absorption spectroscopy). SFG vibrational spectroscopy has two detection schemes, namely, scanning narrow band and multiplex broad band detection [3]. The scanning method usually takes a long time (~tens of minutes, see e.g [8].), has a low density of spectral points, and suffers from the shot to shot noise of the source lasers. Moreover, scanning inevitably leads to the constant displacement of the IR beam spot at the probed interface due to the motion of the nonlinear crystals during tuning; compensation can be introduced but requires elaborate beam steering setups [16]. More recently, Richmond and colleagues reported a study of ion adsorption kinetics at the water/CaF₂ interface by following the SFG intensity in time at two separate IR frequencies [8]. This, however, does not provide a straightforward correlation between the multiple spectral components of the broad OH vibrational spectra in real time.

To overcome problems of the scanning method, multiplex detection is often used in ultrafast spectroscopy. Since its introduction by Richter and colleagues [17], the term “broadband SFG” has typically referred to spectra obtained over a bandwidth of ~200 cm⁻¹ [18]. While this is often enough to cover the entire C-H stretch region for long-alkyl chain surface-ordered systems [19] such as lipids, it is much narrower than the typical hydrogen-bonded OH stretch region extending over several hundred wavenumbers. This limitation is mostly set by the bandwidth of available IR optical parametric amplifiers, resulting from the group-velocity mismatch between interacting pulses in conventional collinear OPA’s.

Broadband SFG spectroscopy can be extended to wider frequency ranges (~700-1000 cm⁻¹) by setting the center of IR pulses to several neighboring frequencies (so-called hybrid scanning-tuning broadband SFG) to cover spectra over a broader region [20,21]. However, this approach is practically limited to acquisition of static spectra, as responses at each central frequency of the IR are recorded sequentially. The most recent commercial OPA-DFG systems can achieve FWHM ~400 cm⁻¹, potentially providing an SFG spectral window of ~700-800 cm⁻¹, and recently the Yan and Tahara groups have shown acquisition of OH stretch spectra from H₂O/air interface without tuning the OPA IR output [22,23]. However, the integration times can be rather long (~15 min) [22] due to low Fresnel factors in external-reflection SFG. Tahara and colleagues obtained spectra within 2 min, thanks to the increased sensitivity of heterodyne-detected sum-frequency [23]. In general, it is desirable to generate ever broader infrared pulses for simultaneous probing of various interfacial oscillator species, to reduce integration times, and in particular to probe ultrafast dynamics at aqueous surfaces on shorter time scales.

In this paper, we propose an alternative approach, extending broadband SFG acquisition to larger bandwidths, ~1000 cm⁻¹ to probe the entire spectrum of the interfacial OH stretches and potentially the CH stretches at mineral surfaces (~2800 – 3800 cm⁻¹). At the same time, we increase considerably the speed of acquisition of vibrational SFG spectra in this important frequency range. The key elements in our setup are: 1) the ultra-broadband IR non-collinear optical parametric amplifier (non-collinear OPA or NOPA, see below) recently developed in our laboratory, combined with 2) total-internal reflection (TIR) geometry SFG probing [4,24,25] and 3) a commercially available low-noise broadband detection system enabling acquisition of SFG spectra with high signal-to-noise ratios (SNR). We demonstrate the acquisition of OH stretch spectra of water at hydrophilic and hydrophobic silica surfaces simultaneously over the frequency range ~2800 – 3800 cm⁻¹ at a single setting of the NOPA and CCD detector (“single-spectrum”, or “single-acquisition” mode). Optimization of the detection sensitivity, combined with the TIR geometry SFG, allow us to perform such spectral

acquisitions within 60 seconds and obtain high-quality vibrational SFG spectra. During the acquisition of the spectrum, no parts of the optical setup mechanically move, as the ultrabroadband NOPA provides the necessary bandwidth to cover the entire OH-stretch frequency range; hence we avoid any issues connected with the beam spot displacement which otherwise may be present in the case of narrowband IR sources.

The paper is organized as follows: in section 2, we consider the basic principles behind ultra-broadband IR noncollinear OPA's. In section 3, we describe the optical setup of our broadband IR NOPA, the TIR SFG setup employed for SFG spectroscopy of silica/water interfaces and characterization of the IR pulses. Finally, section 4 provides the results of the SFG from water at mineral interfaces using the ultra-broadband IR pulses from the NOPA.

2. Broadband optical parametric amplification of infrared pulses

The generation of tunable infrared pulses via optical parametric generation/amplification (OPG/OPA) has become the method of choice for various ultrafast spectroscopies [26,27]. Briefly, OPA is a nonlinear optical process in which a pump photon of frequency ω_p generates and amplifies two photons of lower frequencies conventionally called signal and idler (ω_s and ω_i) [27]. Energy conservation dictates that $\omega_p = \omega_s + \omega_i$, while conventionally $\omega_s > \omega_i$. The use of 800 nm pulses from Ti:sapphire ultrafast lasers as the pump beam in OPA setups enables direct generation of the IR tunable in the $\sim 3 - 6 \mu\text{m}$ region from nonlinear crystals that are phase matchable in the mid-IR region (e.g. KTiOPO_4) [27]. In this case, the mid-IR idler pulses are generated during OPA of near-IR signal pulses ($\sim 1.0 - 1.5 \mu\text{m}$).

Typically, the bandwidths of IR pulses from parametric laser sources (such as commercial collinear OPA's) are limited to several hundred wavenumbers. The main reason for this limitation is the group-velocity mismatch between signal and idler pulses due to the following relation $\Delta\omega_s = \Delta\omega_i \propto |1/v_s - 1/v_i|$ (if the second and higher orders of dispersion are negligible) [26–28]. Such bandwidths, in turn, limit the shortest achievable pulsewidths in the IR to ~ 50 fs [29]. Recent advances in ultra-broadband optical parametric amplification in the near-IR with pump at 800 nm [27,30] have led to much broader near-IR signal and mid-IR idler pulses [31]. Dispersive properties of certain nonlinear crystals, such as potassium niobate, lithium niobate, potassium-titanyl phosphate, lithium iodate etc., create favorable conditions for generation of broadband idler pulses in the $\sim 3\text{-}5 \mu\text{m}$ range [27,31]. These materials have zero group-velocity dispersion (GVD) occurring at wavelengths close to $\sim 1.8 - 2 \mu\text{m}$. Thus, when pumped at 800 nm, there will be pairs of signal-idler wavelengths at which the group velocity of signal matches that of the idler [27]. For materials such as potassium niobate, lithium niobate, potassium-titanyl phosphate, etc., this situation occurs at signal wavelengths $\sim 1000 - 1100$ nm (for the case of collinear OPA). These signal wavelengths correspond to the idler frequencies at $\sim 2500\text{-}4000 \text{ cm}^{-1}$ in a 800-nm pumped OPA [31]. The group-velocity matching results in the increase of signal amplification bandwidth, while the idler pulses generated will be automatically broadband due to energy conservation.

Using this method, the Cerullo group generated $\sim 220\text{-}500 \text{ cm}^{-1}$ broad IR pulses (at FWHM) tunable from ~ 3 to $5 \mu\text{m}$ in lithium iodate, LiIO_3 [31]. The same group later generated even broader mid-IR pulses using a specially designed fan-out periodically poled stoichiometric lithium tantalate (PP-SLT) crystal [32]. Fan-out periodical poling enables fine tuning of the poling period when the crystal is translated normal to the beam direction thereby adjusting the poling period. Pulses stretching from $2.7 \mu\text{m}$ to $>4 \mu\text{m}$ (spectral coverage $>1200 \text{ cm}^{-1}$) were reported, and compression to ~ 25 fs was shown. An alternative method for the generation of broadband IR pulses is via four-wave mixing (FWM) in air [33,34] and more recently in fused silica [35]. However, the efficiency of FWM, a third-order nonlinearity, is orders of magnitude less than for OPA, a second-order nonlinearity.

We have achieved generation of ultra-broadband IR pulses from various configurations of a double-stage non-collinear OPA (at least two stages of OPA are required in order to generate sufficient power of infrared idler for SFG experiments [29,31,36]). However, in

contrast to the above-mentioned experimental setup employing a fan-out PP-SLT, we use nonlinear crystals in their bulk, i.e. monocrystalline, forms. We demonstrated experimentally that nonlinear materials such as bulk potassium-titanyl phosphate (KTiOPO₄, KTP), potassium niobate (KNbO₃, KNB), lithium niobate (LiNbO₃, LNB) also provide conditions for broadband phase matching in the IR [37–40]. More recently, we reported extension of the near-IR NOPA in KTP into the regime of high repetition rates [41]. Bulk crystals are much less expensive than periodically-poled crystals, whose production requires special engineering. In addition, phase matching predictions for periodically-poled materials in some cases are not easily confirmed in experimental OPA setups [42], while for monocrystalline materials phase matching calculations are more straightforward since there is no dependence on the poling period.

Crystals such as LiNbO₃ and KNbO₃, similar to KTP, are suitable for ultrabroadband phase matching in the near-IR [40]. In particular, they have relatively high nonlinear optical coefficients ($d_{22} = 2.46$ pm/V and $d_{31} = -4.64$ pm/V for LNB; $d_{31} = -12$ pm/V for KNB, measured at 1.064 μm for both crystals [43]). LNB and KNB have been used as efficient nonlinear crystals for generation of fs-pulses in the $\sim 2\text{--}4$ μm wavelength region [36,43,44]. Here, we demonstrate generation of broadband IR pulses from a two-stage NOPA based on LNB and KNB crystals and the application to broadband SFG vibrational spectroscopy of water/mineral (SiO₂) surfaces.

3. Experimental setup

The ultra-broadband sum-frequency generation setup for the vibrational spectroscopy of water/mineral surfaces integrates two main components (Fig. 1): 1) ultra-broadband IR non-collinear optical parametric amplifier and 2) total-internal reflection sum-frequency setup combined with a low-noise fiber-collection detection system. They are described below.

3.1. Non-collinear optical parametric amplifier and its spectral characterization

The integrated broadband NOPA-SFG spectroscopic setup is pumped by a custom-built Ti-sapphire regenerative amplifier (Alpha-1000 by BMI-Coherent) operating in fs-mode [45]. The 800-nm beam is split into two parts: ~ 350 mW to pump the broadband IR NOPA and ~ 225 mW to serve as the VIS beam in the sum-frequency measurements. The two-stage 800-nm pumped NOPA incorporates the generation of a broadband near-IR white-light continuum (WLC) seed and its further broadband amplification in two consecutive non-collinear OPA stages.

The KNB crystal (2.46-mm thick, VLOC) is cut for phase matching in ZX-plane (also noted as BC-plane) plane at $\theta = 38^\circ$, and the congruent lithium niobate crystal (c-LNB, 2-mm thick, CASIX) is cut for phase matching in (Z,-Y)-plane at $\theta = 48^\circ$ as described previously [40]. The broadband single-filament WLC beam, generated by focusing few-microjoule 800-nm pulses into a 2-mm thick sapphire plate, was collimated by a silver spherical mirror ($f = 25$ mm). The broadband near-IR seed beam was overlapped with $\sim 50\text{--}100$ μJ of 800-nm beam at the c-LNB crystal. The first NOPA stage provided several microjoule near-IR pulses [40], which were further amplified at the KNB-NOPA stage. To fulfill the phasematching conditions at both nonlinear crystals, the 800 nm pump pulses were horizontally (extraordinary) polarized, while the near-IR signal pulses were polarized in a vertical plane (ordinary). The external non-collinear angle between the signal seed and pump pulses was $\sim 5^\circ$ for KNB-NOPA and $\sim 4^\circ$ for c-LNB-NOPA, corresponding to the internal non-collinear angle $\sim 2.4\text{--}2.5^\circ$ for KNB and $\sim 1.9\text{--}2.0^\circ$ for c-LNB [40]. The non-collinear geometry between the continuum seed and pump at the lithium-niobate crystal enabled generation of ultra-broadband near-IR pulses (bandwidths >1000 cm^{-1} , or ~ 200 nm in the $\sim 1050 - 1600$ nm range) [40]. At each NOPA stage, the pump beam was focused loosely to a point before the crystal as close as possible before the onset of optical parametric generation. Such pump focusing was important, in particular, for the generation of idler beam of a relatively good

spatial quality that could be tightly focused at the probed surface to provide high levels of SFG. The path of the idler beam was traced with a liquid-crystal heat-sensitive card (Edmund Optics). The idler beam was collimated with a 1-inch diameter, $f = 50$ -mm CaF_2 lens and transmitted through a $1.6 \mu\text{m}$ long-pass coated filter (Andover). The polarization of the idler pulses is vertical.

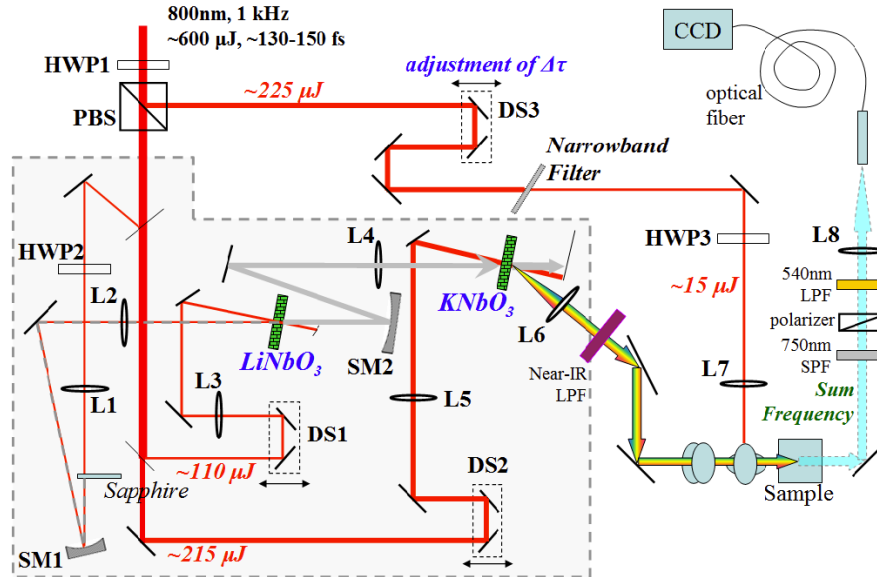


Fig. 1. Optical setup of the LNB-KNB-based double-stage NOPA (area inside of the dashed contour) integrated with the broadband vibrational SFG spectroscopy setup: HWP, half-wave plates; Sapphire, 2-mm thick plate; PBS, polarizer-beamsplitter; LPF, long-pass filters; SM, spherical mirrors (SM1, +25 mm; SM2, +200 mm); L, lenses (L1, BK7, 100 mm; L2, fused silica, 300 mm; L3, BK7, 340 mm; L4, fused silica, 250 mm; L5, BK7, 300 mm; L6, CaF_2 , 50 mm; L7, BK7, 200 mm; L8, BK7, 50 mm); SPF, short-pass filter; DS, delay stages; CCD, Andor integrated charge-coupled device camera with a grating spectrometer. Idler beam is showed with multicolored arrows.

The idler beam generated by the KNB crystal was characterized spectrally by sum-frequency upconversion with 800-nm pulses on a polycrystalline ZnSe (P-ZnSe) plate (Fig. 1) [37,39]. Tuning of the broadband idler pulses was achieved by rotating the KNB crystal over a total external angle of ~ 1 - 2° , corresponding to $\sim 1^\circ$ change of the internal phase-matching angle, which indicates that KNB provided a high angular acceptance. The phase-matching in LNB-crystal was adjusted in parallel. Adjustment of temporal delays between the signal and pump pulses at both crystals was required (especially pronounced for generation of lower-frequency idler spectra), indicating that the near-IR seed underwent temporal stretching in the optical components. For each setting of the NOPA at which the idler spectra were acquired, the idler beam power was measured.

The broadband idler pulses generated from the second KNB NOPA stage (Fig. 2) could be tuned over a wide frequency range $\sim 2800 - 6000 \text{ cm}^{-1}$. The spectrum centered at $\sim 3400 \text{ cm}^{-1}$ covers $>1000 \text{ cm}^{-1}$ (FWHM $\sim 700 \text{ cm}^{-1}$). Such a broad spectrum should support transform-limited pulse durations on the order of ~ 20 fs.

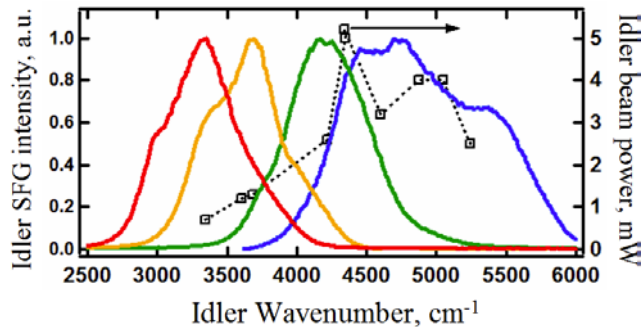


Fig. 2. Broadband idler spectra from the LNB-KNB-NOPA shown in Fig. 1, measured via sum-frequency generation on the polycrystalline ZnSe plate with narrowband 800 nm pulses [39].

A possible reason for the bandwidth narrowing of the idler pulses at $\sim 3400\text{ cm}^{-1}$, compared to 5000 cm^{-1} , could be a larger chirp of the near-IR pulses at the corresponding wavelengths $\sim 1050 - 1250\text{ nm}$. Estimations of group-delay dispersion based on propagation of near-IR pulses through 5 mm of silica and 2 mm of lithium niobate yield $\text{GDD} \sim 0.1\text{ fs}^2/\text{mm}$ at 1100 nm, and $\sim 0.057\text{ fs}^2/\text{mm}$ at 1350 nm. The effect of the chirp of white-light is practically eliminated for idler generation at higher frequencies ($\sim 4000 - 6000\text{ cm}^{-1}$), corresponding to the signal wavelengths $\sim 1300 - 1500\text{ nm}$, at which the group velocity dispersion of sapphire and fused silica is practically zero. Nevertheless, the bandwidth of the 3300 cm^{-1} ($3\text{ }\mu\text{m}$) centered IR pulses was sufficient for the sum-frequency spectroscopy of aqueous interfaces (see below). Note also that the spectra generated from this configuration of NOPA are smoother than the broadband idler from the two-stage KTP-NOPA with divergent seed [39]. Generation of idler down to $\sim 2200\text{--}2500\text{ cm}^{-1}$ ($>4\text{ }\mu\text{m}$) is, in principle, expected from potassium niobate [31,36]; a possible reason that we were not able to tune the idler further into the IR was the increased angular divergence of the idler at longer wavelengths [28], which lead to the inability to collect the longer wavelengths with our present setup. The temporal characterization of the broadband idler pulses at the probed interface is described below in sub-section 3.3.

3.2. Experimental setup for ultra-broadband SFG spectroscopy of silica/water interfaces

For the increased signal-to-noise ratio and improved sensitivity, we perform SFG spectroscopy in the total-internal reflection geometry [4,24,25]. Practically, TIR is achieved by sending the IR and VIS beams above the critical angle through a hemicylinder prism whose flat surface is in contact with the aqueous samples (Fig. 3). For the broadband spectroscopy of silica/water interfaces, the VIS pulses at 800 nm were obtained by splitting off a part of the regenerative amplifier output (Fig. 1). The visible pulses were synchronized with the IR pulses at the sample interface by means of a mechanical translation stage (DS3 in Fig. 1). The polarization of the IR idler beam is in the vertical plane, and the periscope was adjusted such that the IR beam polarization is p (in the plane of incidence) at the probed interface. The polarization of the VIS beam at the interface (s- or p-) was adjusted by a half-wave plate (HWP3 in Fig. 1). The broadband IR beam was focused at the sample surface tightly using a $f = 50\text{ mm}$ CaF_2 lens with diameter $\sim 10\text{ mm}$ (not shown). The VIS beam was focused at the probed surface loosely with a $f=200\text{ mm}$ BK7 lens (L7 in Fig. 1). The VIS beam was focused before the silica prism; the focal point was as close as possible to the prism to maximize the reference SFG signal from the gold-coated fused silica prism before the onset of continuum generation in the bulk of the prism samples. Based on the diameters of the IR ($\sim 2\text{ mm}$, as observed on the thermosensitive card) and VIS beams ($\sim 3\text{ mm}$) we estimate the diameters of the beams (assumed as Gaussian) at the probed surface to be $\sim 95\text{ }\mu\text{m}$ and $195\text{ }\mu\text{m}$

respectively. Based on these estimated values and the angles of incidence, the pulse peak intensities at the interface were estimated to be $\sim 4.8 \text{ GW/cm}^2$ for IR beam and $\sim 40 \text{ GW/cm}^2$ for VIS beam respectively. Note that since the IR beam has a pulse front tilt due to angular dispersion, the actual spot size can be larger. The tight focusing of the IR beam allowed the spatial overlap of various colors within the broadband IR pulse with the larger-spot visible beam.

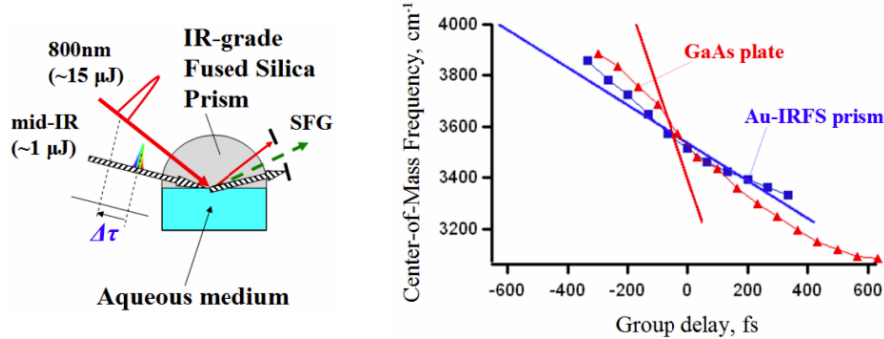


Fig. 3. Left: schematic of the beam geometry in our SFG-spectroscopy setup. Right: Measurement of the chirp in the broadband IR pulses at the sample surfaces with femtosecond 800 nm pulses. Red triangles: center-of-mass (COM) frequencies of the IR pulses measured on a GaAs plate in the SFG-setup vs IR-VIS pulse delay. Blue squares: COM's measured on the Au-IRFS reference prism. Red solid line: calculated group delay for the case of $\sim 3300 \text{ cm}^{-1}$ centered pulses propagated through (2-mm KNbO_3 +5-mm CaF_2). Blue solid line: calculated group delay for the case of $\sim 3300 \text{ cm}^{-1}$ centered pulses propagated through (2-mm KNbO_3 +5-mm CaF_2 +12-mm fused silica). Red and blue thin dotted lines are guides for the eye.

The IR-grade fused silica (IRFS) hemicylinder prisms (Fig. 3) were 0.5 inch in radius (ISP Optics). The incidence angle of the VIS beam was set very close to the critical value. For the silica/water interface, the critical angles are $\sim 66^\circ$ for 800 nm, $\sim 66^\circ$ for SFG over the range ~ 618 – 645 nm , and change from $\sim 63.5^\circ$ to $\sim 65^\circ$ for the IR beam over the range ~ 3100 – 3700 cm^{-1} (calculated by the real part of the index of refraction). The incidence of the 800 nm beam was set to be just above the critical angle (by observing the reflection of 800 nm from silica/water surface) at $\theta_{\text{VIS}} \sim 67^\circ$. The IR beam incidence angle was estimated to be $\sim 75^\circ$. Such beam geometry enables optimal signal levels due to the TIR of the VIS and sum-frequency beams, while the off-critical incidence of the IR beam suppresses the Fresnel factor dependence on the frequency due to the water absorption [24,25]. The IRFS hemicylinders (sample and the gold-coated reference prisms [19,46], see below) were placed onto a Teflon sample holder sitting on a XYZ translation stage. The water/silica interface was created by placing the prism on top of aqueous samples inside the cell [46].

The collection and collimation of the SF-beam generated at the sample interface was done with a 2-inch diameter $f=70 \text{ mm}$ lens. The SFG beam was filtered with three 750-nm short-pass filters (Melles-Griot) which completely suppressed the otherwise overwhelming and ubiquitous 800-nm pulses. The SFG beam was focused into the fiber input with a 50-mm lens. The polarization of the probed sum-frequency beam at the interface (s- or p-) was selected by a polarizer in front of the fiber input (Fig. 1). The use of fiber coupling suppressed significantly the contribution of stray light compared to free beam propagation. The fiber sent the SF-signal to an Andor spectrograph+CCD integrated detection system via a fiber-adaptor (spectrograph: model “Shamrock” based on a 500 nm blazed grating, 600 grooves/mm; CCD: low-noise thermo-electrically cooled detector, model iDus DU401A-BV, maximum quantum efficiency ~ 80 – 90% at ~ 550 – 600 nm). The dispersion of the grating allowed observation of the sum-frequency response from 500 nm to $>650 \text{ nm}$ at once, providing resolution of $\sim 1 \text{ nm}$ ($\sim 28 \text{ cm}^{-1}$ at 600 nm).

3.3. IR pulse characterization on Au-coated prism

To characterize the spectra of the IR pulses at the probed silica surfaces, we used a gold-coated infrared-grade fused silica prism [19] (Au-IRFS), which was prepared by vacuum deposition on IR grade fused silica hemicylindrical prisms identical to those used for silica water experiments. Temporal characterization of the infrared pulses was done by cross-correlation with unstretched ~ 130 fs 800-nm pulses. The IR pulses arrive at the probed interface considerably chirped as evident from the appearance of different components of the ultra-broadband SFG pulse at different IR-VIS pulse delays (Fig. 3). In principle, the fused silica prism is expected to add a considerable chirp of the IR pulses: ~ 10 mm of silica path for the IR beam corresponds to group delay dispersion of $-533 \text{ fs}^2/\text{mm} \times 10\text{mm} \sim -5330 \text{ fs}^2$ calculated at $\sim 3300 \text{ cm}^{-1}$, resulting in a chirp of $\Delta\tau \approx \text{GDD} \cdot (2\pi\Delta\nu) \approx 1000$ fs for pulses with a $\Delta\tilde{\nu} \approx 1000 \text{ cm}^{-1}$ bandwidth [47].

Interestingly, the measurements of chirp within the IR pulses with femtosecond 800 nm pulses showed that the temporal stretching effect of the fused silica prism did not make a significant contribution to the overall chirp in the IR pulses, as compared to the chirp measured on a bare GaAs plate (Fig. 3). This indicates that other effects, such as the angular dispersion of the IR idler beam generated in a non-collinear OPA configuration [28], make even more significant contributions to the observed temporal chirp of the IR pulses. Briefly, the idler pulses generated from a NOPA possess considerable angular dispersion and pulse-front tilt [28,38,48] inducing elongation of the pulse duration at the focus which can be calculated [49]. Our estimations of the IR pulse durations at the probed interface due to tilting yield values ~ 1.3 - 1.7 ps, close to the experimental observations (Fig. 3). Additional proof for such an explanation is that the chirp of the IR pulses measured on the GaAs plate (Fig. 3, red triangles) is considerably larger than the chirp expected from dispersion introduced into IR pulses by 2 mm of KNbO_3 and 5 mm of CaF_2 (collimating and focusing lenses) [50] (Fig. 3, red solid line).

Inclusion of few mm total of silicon plates into the IR beam path [50] did not significantly decrease the chirp of IR pulses, most likely due to the angular dispersion of the broadband IR idler pulses [28]. A possible approach to suppress the angular dispersion in the IR would be by retracing and collimating the colors within the broadband idler beam with the help of a dispersive grating [28]. However such an approach would considerably decrease the idler pulse energy which is essential for SFG (where low intensity signals are typical). For example, the idler energy losses were on the order of ~ 65 - 70% in the previous reports on ~ 400 -nm pumped BBO-NOPA [28,48]. The idler pulses can be generated from the collinear OPA, however, the bandwidth of the IR pulses would be sacrificed. Thus the ultra-broadband spectroscopy of the aqueous interfaces was performed with the idler beam directly from the NOPA, without correcting the angular dispersion.

In order to improve the temporal overlap of the chirped broadband IR pulses and visible pulses, and at the same time to improve the resolution of spectral acquisition, the 800 nm beam was passed through an interference narrowband filter [18] (Fig. 1). The filter narrowed the VIS pulse spectrum to ~ 2 - 2.3 nm and consequently stretched the pulse duration to ~ 500 fs [18] (not measured in the present work). The transmitted central frequency, together with the transmitted beam power, was adjusted by rotating the narrowband filter around a vertical axis. The visible pulse energy decreased from ~ 220 to ~ 15 μJ after narrowing in the filter. After insertion of the narrowband filter, the spectral bandwidth of sum-frequency signal that could be observed simultaneously from Au-IRFS reference prism, significantly increased (from $\sim 200 \text{ cm}^{-1}$ at each value of interpulse delay with fs-VIS pulses to $>600 \text{ cm}^{-1}$ FWHM with stretched VIS pulses in the $\sim 3200 - 4000 \text{ cm}^{-1}$ range). These spectrally narrowed visible pulses were used in all of our ultrabroadband surface vibrational SFG studies.

The SFG wavenumber scale calibration was performed by measuring spectra off the gold-coated fused silica prism with a ~ 1 -mm thick quartz plate in the IR beam path. The latter has

an intense and relatively narrow, for the current measurements, absorption peak at 3672 cm^{-1} (corresponding to the O-H stretch vibrations of the bulk silanols). The frequency of the SF spectra was offset to match the location of the dip in the IR absorption peak position [22].

4. Acquisition of vibrational SFG spectra of interfacial water with broadband IR pulses

The infrared-grade fused silica prisms used for the broadband vibrational spectroscopy of mineral/water interfaces were prepared by cleaning in “piranha” cleaning solution which is 1 vol. conc. H_2O_2 ; 3 vol. conc. H_2SO_4 (CAUTION: “piranha” is a very reactive and corrosive mixture! It must be handled with a great care; use of protective equipment such as gloves, eye goggles and labcoat is mandatory.). The hydrophobic silica surface was prepared by immersing a fused silica prism into a solution of octadecyltrichlorosilane $\text{CH}_3(\text{CH}_2)_{17}\text{SiCl}_3$ (OTS) which would coat the prism surface with a monolayer of long-chain hydrocarbon [19]; this prism is referred to as OTS-IRFS. Water was obtained from a Thermochemical Barnstead Easypure II purification system equipped with a UV lamp; final water resistivity $\sim 18\text{ MOhm}\cdot\text{cm}$. D_2O , 99.9% D, Cambridge Isotope Laboratories, was used as received.

Due to the chirp of the IR pulses at the silica/water surface, the IR-VIS interpulse delay $\Delta\tau$ had to be progressively scanned in order to upconvert the entire spectrum of the broadband IR pulses (Fig. 4a). The sum-frequency spectra of the water/silica surface changed accordingly with the time delay $\Delta\tau$. We acquired the spectra over the entire spectral range of the broadband IR by scanning the VIS-IR pulse delay $\Delta\tau$ (Fig. 4b). The SFG spectra were acquired from both the Au-IRFS reference prism and fused silica sample prisms at the same delays. As the visible pulse upconverted various parts of the broadband IR spectrum, the vibrational features at corresponding frequencies appeared in the SFG spectra at the corresponding delays (Fig. 4). For the example of SFG-spectra from water/hydrophobic silica (Fig. 4), at earlier delays (higher frequencies are upconverted), there is a peak at $\sim 3700\text{ cm}^{-1}$ which we assign to non-hydrogen bonded water molecules. At long delays (lower frequencies are upconverted) peaks in the region $\sim 2850\text{-}2950\text{ cm}^{-1}$ are clearly observed. The latter features correspond to symmetric and asymmetric stretches of the terminal CH_3 and CH_2 groups in the monolayer [15,19]. These peaks are broadened since the resolution of the present setup is not enough to resolve these peaks separately.

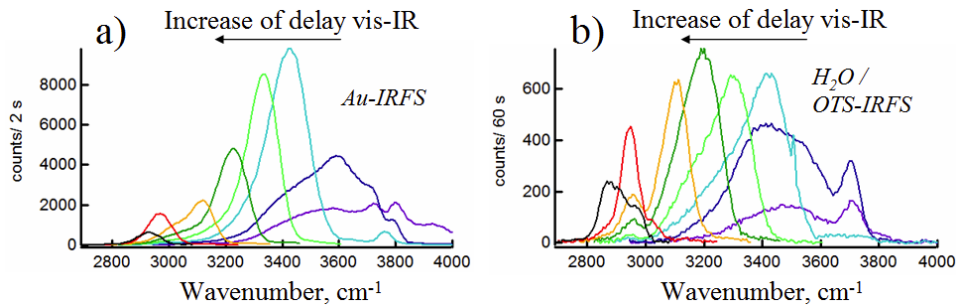


Fig. 4. Acquisition of sum-frequency spectra from silica (OTS-IRFS)/water interfaces by scanning the VIS-IR delay $\Delta\tau$ [15]. (a) ppp SF-spectra from Au-IRFS prism at selected VIS-IR delays (spectra are shown spaced at 267 fs); (b) ppp-SF-spectra from $\text{H}_2\text{O}/\text{OTS-IRFS}$ prism at the same selected values of $\Delta\tau$ as for the Au-IRFS reference prism in a).

Even with the chirp present in the IR pulses, our ultrabroadband NOPA-SFG setup allowed us to routinely acquire spectra from the silica/water interface in the TIR geometry. We overcame the chirp of the IR pulses and measured the vibrational SFG spectra of OH stretches over the $3000 - 4000\text{ cm}^{-1}$ region by two approaches:

- 1) integration of the spectra from the aqueous interfaces obtained at a series of values of the delay, $\Delta\tau$, and normalization by the sum of spectra from the gold-fused

silica prism measured at the same delays. This approach allowed acquisition of vibrational SFG spectra with high signal-to-noise ratios.

2) optimization of the temporal and spectral overlap of the IR and VIS pulses (occurring mostly at the earlier values of $\Delta\tau$, Fig. 4). This approach allowed acquisition of water/silica sum-frequency spectra at a single value of $\Delta\tau$, within a single CCD camera acquisition.

These two approaches are described in more detail below.

Approach 1. Scanning of the VIS-IR pulse delay

The separation between delays (increment) at which SFG spectra were acquired was typically ~ 133 fs. At each corresponding value of $\Delta\tau$, the sum-frequency spectrum was acquired from the gold reference prism and from aqueous samples. For the case of beam polarizations at the interface SFG = p, VIS = p, IR = p (notation ppp), the typical integration times at each fixed delay value were ~ 1 -2 s for gold-silica prism and ~ 30 -60 s for aqueous/silica interfaces. For the beam polarizations SFG = s, VIS = s, IR = p (notation ssp), the integration times at each fixed delay value were ~ 20 s for gold-silica prism and ~ 30 -60 s for aqueous/silica interfaces. The spectral shapes of the vibrational sum-frequency spectra from neutral H₂O/silica surface in the two polarization schemes were very close. However, in ppp the signal-to-noise ratio was much higher than in ssp. Thus, for silica/water interfaces, we carried out the measurements with the ppp polarization scheme [4].

The spectra from the hydrophilic silica/water surface and hydrophobic OTS-silica/water interface (Fig. 5) show spectral features that are in good agreement with the previously reported spectra. In particular, we are able to reproduce the double-peak structure of the water-silica sum-frequency spectra (peaks at ~ 3200 and ~ 3450 cm⁻¹) reported previously [1]; in addition, we observe the disappearance of the sum-frequency signal upon replacing H₂O with D₂O (Fig. 5a, green), which proves that the signal originates from the vibrations of OH-oscillators at the probed interface. The robustness of the SFG-spectrum acquisition was assured by the reproducibility of the water/silica interface spectrum.

We are also able to reproduce the main features of the sum-frequency spectra of water molecules at a hydrophobic interface (Fig. 5b). These features are namely the broad peak(s) corresponding to hydrogen-bonded OH-vibrations (~ 3100 – 3500 cm⁻¹; dominant in the SFG spectra at hydrophilic interfaces), and the much narrower, so-called “free-OH”, or “dangling OH” peak (~ 3700 cm⁻¹) corresponding to non-hydrogen bonded OH-oscillators [14,15] (Fig. 5b).

As mentioned above, the use of TIR geometry for SFG spectroscopy, together with the 30-60 sec integration times provided large signal-to-noise ratios (SNR) of the vibrational SFG spectra, especially in the ppp configuration. Similarly to the work by the Yan group [22], we estimated the SNR of the normalized sum-frequency spectra as the ratio of the maximum of the resonant OH signal to the RMS of noise oscillations (which can be accessed by measuring SFG of D₂O/fused silica, see green line in Fig. 5 (a)). Calculated in such a way, the SNR values were on the order of ~ 2000 for the neutral H₂O/fused silica surface, and ~ 200 for neutral H₂O/OTS-IRFS interface, while in the ssp polarization configuration, the typical SNR values for neutral H₂O/fused silica surface were >20 which is ~ 2 x improvement compared to the previous measurements. An additional factor that lead to such high SNR values is the relatively low noise of the iDus Andor CCD. The high SNR of this integrated broadband-NOPA-SFG setup enabled us, in particular, to systematically observe and study a feature at ~ 3700 cm⁻¹, (Fig. 5a) in the spectra of the silica/water interface, which will be discussed elsewhere.

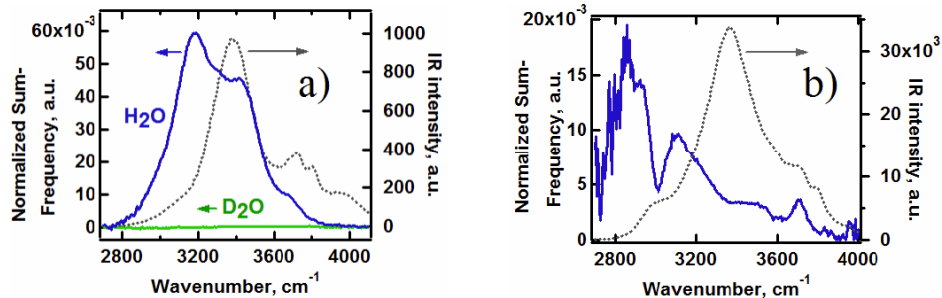


Fig. 5. (a): Normalized SFG-spectrum of the neat fused silica/neat water (pH~6) interface (blue solid line) in ppp-polarization, shown together with the reference spectrum of the ultra-broadband IR pulses (dotted grey line). The green solid line is the SFG spectrum from the neat fused silica/D₂O interface shown on the same scale with the H₂O/fused-silica spectrum. (b): Normalized SFG-spectrum of OTS-coated silica / neat water (pH~6) interface (blue solid line) in ppp-polarization, together with the reference spectrum of the ultra-broadband IR pulses (dotted grey line).

Interestingly, even though the relative intensity of the broadband IR pulses is rather low at $\sim 2900\text{ cm}^{-1}$, we are still able to observe the C-H stretches of the methyl groups within the OTS-monolayer in the $2800 - 3000\text{ cm}^{-1}$ range (Fig. 5b). Since the current SFG setup was optimized for the spectroscopy of the broadband spectral features of OH, its resolution ($>35\text{ cm}^{-1}$) was rather poor to study such spectrally narrow features as C-H stretches in OTS-monolayers (natural linewidths $\sim 10\text{ cm}^{-1}$ or less) [19], and thus the SF-spectroscopy of these modes was not pursued in detail in the current work.

Approach 2. Sum-frequency acquisition from silica/water interfaces in single-spectrum mode

The acquisition of SFG spectra from silica/water interfaces was reliably and reproducibly obtained by adjusting the delay between the ultrabroadband IR pulses and the visible pulses to compensate for the chirp in the IR pulses. We were able also to implement acquisition of SFG spectra of OH stretches in the entire spectral range even without tuning the IR-VIS delay, i.e., in a single spectrum acquisition of the CCD detector. With the spectrally narrowed VIS pulses, the broadest spectral range of the IR pulses overlapped simultaneously with the VIS pulses occurs at earlier delays (Fig. 4). At lower frequencies, the temporal chirp increases, most likely due to the increased dispersion of the materials and larger angular dispersion at longer idler wavelengths. Still, we were able to adjust the interpulse delay and the IR pulse spectrum so that the broadest spectral range of the IR pulses is upconverted at once and the intensities of the SFG signal from the reference sample in the wings of the spectrum are balanced.

To test the applicability of such an approach to the acquisition of SFG spectra of interfacial water, we first acquired a spectrum from a sample interface, for example H₂O at OTS-fused silica at a single delay (Fig. 6). Then, the spectrum was compared to that obtained by scanning the IR-VIS delay, as described in the previous sub-section. The normalization of the spectrum obtained in the single-spectrum mode was done using the reference SFG spectrum obtained from the Au-IRFS prism at the same IR-VIS delay.

Similar to the hydrophobic OTS-fused silica surface, the spectra from water at hydrophilic fused silica could be obtained in the “single-spectrum” mode as well (Fig. 7). For each of the systems, i.e., water at hydrophilic and hydrophobic silica surfaces, the correspondence between the spectrum obtained in a single CCD acquisition and the spectrum obtained by scanning the IR-VIS delay was remarkably good. In the C-H stretch region the agreement between delay-scanning and single-acquisition spectra for the water spectra at the

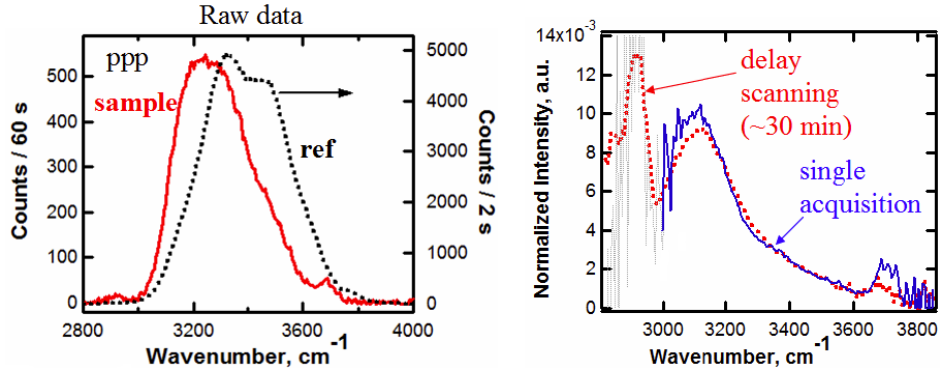


Fig. 6. Left: raw spectra obtained at a single IR-VIS delay from the H₂O/OTS-IRFS interface (“sample”, red) and the gold-coated IRFS (“ref”, black). The sample spectrum was acquired in 60 sec. Right: “single-acquisition” SFG spectrum of H₂O/OTS-IRFS interface (blue) obtained by normalizing the “sample” spectrum in the left-hand side graph by the “ref” spectrum. Red dotted line in the background – SFG spectrum from water/OTS interface obtained by integrating SF-signal as the delay between IR and visible pulses was scanned. For convenience, the single-acquisition spectrum is truncated at ~3000 cm⁻¹ due to the large noise in the C-H stretch region (grey dotted line).

OTS-coated silica was rather poor. The intensity of the SFG signal which is upconverted at this frequency was low indicating insufficient temporal overlap between IR and VIS pulses at ~2900 cm⁻¹. Due to this, SFG spectra from H₂O/OTS-IRFS in “single-acquisition” mode typically had large noise levels below 3000 cm⁻¹, and CH modes could not be clearly seen (Fig. 6). On an additional note, the correspondence between “single-acquisition” SFG spectra and those obtained by scanning the IR-VIS interpulse delay suggests that the relaxation of vibrational coherence between the OH oscillators occurs faster than the duration of the narrowband VIS pulse.

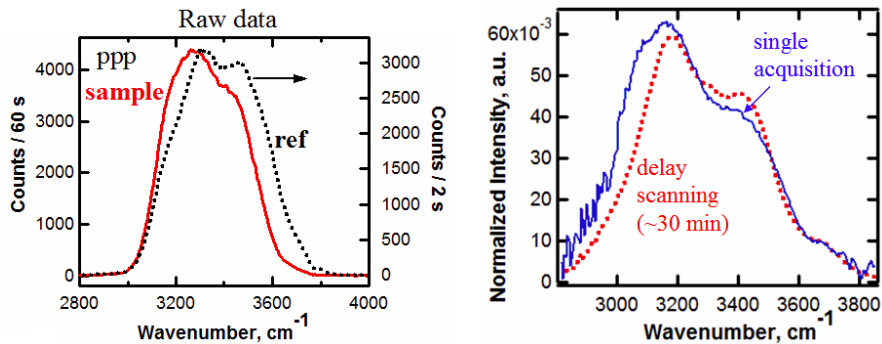


Fig. 7. Left: similar to Fig. 6, raw spectra obtained at a single IR-VIS delay from the H₂O/bare IRFS interface (“sample”, red) and the gold-coated IRFS (“ref”, black). The sample spectrum was acquired in 60 sec. Right: “single-acquisition” SFG spectrum of H₂O/bare IRFS interface (blue) obtained by normalizing the “sample” spectrum in the left-hand side graph by the “ref” spectrum. Red dotted line in the background – SFG spectrum from water/bare silica interface obtained by integrating SF-signal as the delay between IR and visible pulses was scanned.

In conclusion, we have developed an ultra-broadband infrared NOPA and applied it to broadband sum-frequency vibrational spectroscopy of OH oscillators at mineral/water interfaces. The NOPA setup is relatively simple due to the use of bulk, rather than periodically poled, nonlinear optical crystals. The use of TIR-geometry for SFG acquisition, combined with the low-noise detection system enables collection of high-SNR spectra, while the broad bandwidth of the NOPA provides SF-vibrational spectra of the entire OH-stretch

region without tuning the IR pulses. For single-spectrum acquisition, SNR values on the order of 100-120 for H₂O/neat silica (Fig. 7) and ~35 for H₂O/hydrophobic silica (Fig. 6) can be obtained in relatively short integration times (≤ 60 sec). These values compare well to the work by the Yan group where SNR~170 was shown from the air/water interface (15 min integration time, external reflection SFG; 203 mW 800 nm, 12 mW IR at 5 kHz) [22]. The high sensitivity of our SFG setup is achieved due to the TIR geometry. However, in order for our broadband NOPA to be applicable to SFG spectroscopy in external reflection geometry (to study e.g. air/water and other interfaces), the infrared output energy should be scaled up to ≥ 10 μ J and/or the integration time increased. This can be achieved by employing several pre-amplification NOPA stages to generate broadband near-IR pulses that would seed the final NOPA stage producing broadband infrared idler pulses.

The relatively short integration time (1 minute) of our device should enable studies of kinetic processes at interfaces on short time scales. Recent developments in the generation of broadband IR pulses at high repetition rates [41,51] have the potential to decrease the integration times even further without sacrificing the SNR. Additionally, if the IR pulses are corrected for their angular dispersion and the chirp, our spectrometer should have the potential to probe ultrafast dynamic processes involving interfacial species occurring on the time scale of tens of femtoseconds.

Acknowledgments

The authors acknowledge the National Science Foundation (grant number CHE 0809838) and the donors of the American Chemical Society Petroleum Research Fund for support of this research. The authors thank Dr. Satoshi Nihonyanagi (Molecular Spectroscopy Laboratory, RIKEN, Japan) for helpful suggestions on the manuscript and Professor Robert Stanley (Temple University, Philadelphia, Pennsylvania) for the loan of his detection system for the initial sum-frequency experiments.